ELSEVIER

Journal of Power Sources 73 (1998) 204–215

JOURNAL OF POWER SOURCES

Predicting lead–acid battery electrode performance using finite difference equations

Rick L. Cantrell *, Dean B. Edwards, Pritpal S. Gill

University of Idaho, Moscow, ID 83843, USA

Received 5 May 1997; revised 7 November 1997

Abstract

This paper presents a computer model that includes the effects of paste conductivity and electrolyte diffusion on the capacity of lead acid batteries. The model simulates the discharge of a complete cell by using finite difference equations to represent electrolyte diffusion in the positive and negative plates as well as in the space between them. The critical volume fraction relates the maximum amount of active material that can be reacted before the paste conductivity limits the reaction. The model uses this and other physical parameters to predict cell capacity. These predictions are then compared with experimental results.

Keywords: Battery; Model; Lead–acid; Electrode; Capacity; Finite difference

1. Introduction

The performance of lead–acid batteries is affected by a number of mechanisms. At low discharge rates, the conductivity of the positive active material limits the battery capacity as lead–sulfate is formed [1–3]. At higher discharge rates, however, the reaction is limited by the slow diffusion of sulfate ions [4–7]. In an attempt to better understand lead–acid batteries, a computer model was developed that incorporates both of these capacity-limiting mechanisms.

Other diffusion models that predict the behavior of lead acid batteries have already been reported by a number of researchers [5–8]. Stein [5] and Horvàth et al. [6] both investigated electrolyte diffusion using Fick's laws. Stein also developed empirical boundary conditions for the electrolyte interface at both the positive and negative plates. Ekdunge and Simonsson [7], experimentally studied the discharge behavior of porous lead electrodes. Ekdunge [8] also developed an integral mean value model that simplified the analysis of the concentration and potential gradients in the electrode.

Many researchers have also studied the effect paste conductivity has on the performance of lead–acid batteries [1,9–12]. Metzendorf [1] studied the dramatic change that occurs after a certain amount of the active material has reacted. Once this amount, which Metzendorf termed the critical volume fraction, is reached the paste becomes largely non-conductive and the reaction comes to a stop. An aggregate-of-spheres model was developed by Winsel et al. [9] and Winsel and Bashtavelova [10] that treats the positive plate as a porous electrode consisting of interconnected spherical particles. Edwards and Appel developed a model [11] to study the conductivity of lead–acid battery electrodes during low rate discharges. In his paper, he also studied the effects of non-conductive glass microsphere paste additives on the critical volume fraction.

Previous modeling at the University of Idaho includes models developed by Appel [13], Gill [14], and Cantrell [15]. Appel used a MacLaurin series expansion to predict the acid concentration within the positive plate, and finite difference equations to model the acid concentration between the positive and negative plates. Gill improved his model by using finite difference equations both between the plates and within the positive plate to estimate the acid concentration. Cantrell took the model one step further by including the negative plate.

The model now includes finite difference equations for both the positive and negative plates, as well as the electrolyte between the plates. Conductivity and diffusion

* Corresponding author.

limiting effects are used by the model to accurately predict the cell performance for a wide range of discharge rates.

The model produces voltage vs. time curves, capacity curves, and acid concentration plots. Capacity curves show the amount of reacted active material as a function of the discharge rate. The acid concentration plots show the acid distribution within the cell over time. The model predictions are compared to experimentally gathered data previously reported [16].

The model presented here is helpful in understanding the behavior of lead–acid batteries. It can also be a useful tool in developing a cell design. A designer can specify plate and cell parameters for an initial design. The model can then be used to determine the cell's performance and, after evaluating the results, the designer can change the parameters in an attempt to meet the desired specifications. A number of iterations can be performed before the first cell is fabricated and tested, saving considerable time and money.

In Section 2, we derive the equations used in the model. In Section 3, we compare the model results with previously reported experimental data [16]. In Section 4, we provide a summary of our results and our recommendations.

2. Model development

In this section, we derive the finite difference equations that serve as the basis for the model. We adapt the general solution to our problem by applying the necessary boundary conditions. Once all of the finite difference equations are developed, they can be placed in matrix form and solved.

2.1. General finite difference equations

The partial differential equation governing the electrolyte concentration within the cell is:

$$\frac{\partial C}{\partial t} = -\frac{\partial J}{\partial x} + \dot{C}_{\mathrm{p}} \tag{1}$$

where C is the molar concentration, J is the ionic flux, t is time, x is position, and the term $\dot{C}_{\mathrm{p}}$ gives the mass generation per volume, $\dot{m}(x,t)/\Delta x \cdot \Delta y \cdot \Delta z$. This equation assumes that the diffusion is one-dimensional in the x-direction. From Fick's first law of diffusion, we get the following relationship:

$$J = D\frac{\partial C}{\partial x} \tag{2}$$

which means that the flux of ions past a perpendicular plane is directly proportional to the concentration gradient across that plane. The term D is the steady-state diffusion rate. The model assumes that the diffusion coefficient is a constant independent of acid concentration. When Eq. (2) is substituted into Eq. (1), the final equation is the modified form of Fick's second law:

$$\frac{\partial C}{\partial t} = -D\frac{\partial^2 C}{\partial x^2} + \dot{C}_{\mathrm{p}} \tag{3}$$

Eq. (3) is the general partial differential equation (PDE) applicable both between the plates and within the positive and negative plates. However, between the plates there is no ion consumption or production so the $\dot{C}_{\mathrm{p}}$ term is equal to zero.

To write the finite difference equations corresponding to the PDE of Eq. (3), the system of nodes shown in Fig. 1 is used. As the figure shows, nodes 1–30 comprise half of the negative plate. Only half of the plate needs to be modeled due to symmetry about the mid-plane. Nodes 31–70 represent the electrolyte between the plates and nodes 71–100 characterize half of the positive plate. Note that the spacing between the nodes in each of the three sections (Δx_{n}, Δx, and Δx_{p} for the negative plate, electrolyte, and positive plate, respectively) is not necessarily the same. For typical cell designs, the nodes within the plates are closer together than those between the plates, giving better results inside the plates where accuracy is more important.

To derive the finite difference equations, the Crank–Nicolson method [17] is used. This method is used because it is second-order accurate in both time and space. This accuracy is achieved by developing the difference approximations at the midpoint of the time increment. This method also provides for a stable, convergent solution.

2.2. General finite difference equation between the plates

Between the plates, the $\dot{C}_{\mathrm{p}}$ term is equal to zero which simplifies the PDE in Eq. (3) to:

$$\frac{\partial C}{\partial t} = -D\frac{\partial^2 C}{\partial x^2} \tag{4}$$

The general finite difference equation that applies between the plates becomes:

$$-\lambda C_{i-1}^{l+1} + 2(1+\lambda)C_i^{l+1} - \lambda C_{i+1}^{l+1} = \lambda C_{i-1}^{l} + 2(1-\lambda)C_i^{l} + \lambda C_{i+1}^{l} \tag{5}$$

where $\lambda = (D \cdot \Delta t)/(\Delta x^2)$, i is the node position, l is the beginning of the time step, and $l+1$ is the end of the time step.

2.3. General finite difference equation within the plates

Inside the plates, the $\dot{C}_{\mathrm{p}}$ term is not zero. Therefore Eq. (3) is the appropriate PDE and is given again for the reader's convenience:

$$\frac{\partial C}{\partial t} = -D^*\frac{\partial^2 C}{\partial x^2} + \dot{C}_{\mathrm{p}}(3) \tag{3a}$$

The diffusion rate, D^*, used here is related to the diffusion constant used between the plates, D, by the equation:

$$D^* = \frac{D}{\tau} \tag{6}$$

This new diffusion rate is defined to account for the possibility of variable tortuosity, τ, within the plates. The tortuosity determines the distance over which the ions must diffuse by affecting the shape of the path. A tortuosity value greater than one increases the diffusion path length and effectively decreases the diffusion rate. For our derivation, the tortuosity of the plates was set equal to one.

The mass generation per volume term used in Eq. (3) can be written as:

$$\dot{C}_{\mathrm{p}} = \frac{\dot{m}_i(x,t)}{\rho_{p,n} \cdot A \cdot \Delta x_{p,n}} \tag{7}$$

where A is the cross-sectional area of the plates, $\Delta x_{\mathrm{p,n}}$ is the node spacing of either plate (shown in Fig. 1), $\rho_{\mathrm{p,n}}$ is the percent porosity of either plate, and $\dot{m}_i(x,t)$ is the rate of ion consumption at each node i. The denominator of the equation above represents the electrolyte volume (pore volume) associated with each node in a particular plate.

To find the $\dot{m}_i$ term needed for Eq. (7), an expression has been developed based on the discharge current and the decrease in concentration per unit of charge transport. The total discharge current is supported by the sum of currents at each of the individual nodes. The current drawn from each node is based on the ion consumption and the resulting change in concentration at that node. The $\dot{m}_i$ term can be written as a function of the current drawn from each node, I_i, and the change in concentration per unit of charge transport, $\partial H/\partial Q$. At the positive plate, this is written as.

$$\dot{m}_i(x,t) = I_i(x,t)\left(\frac{\partial H}{\partial Q}\right)_+ \tag{8}$$

A similar equation is written for the negative plate using $(\partial H/\partial Q)_-$. To determine the values of $\partial H/\partial Q$, the following overall equations for the reactions at the positive and negative electrodes are used [5].

$$\begin{aligned}&+\text{pole:}\\ &\mathrm{PbO_2 + 2e + HSO_4^- + 3H^+ \Rightarrow PbSO_4 + 2H_2O}\end{aligned} \tag{9}$$

$$\begin{aligned}&-\text{pole:}\\ &\mathrm{Pb + HSO_4^- \Rightarrow PbSO_4 + H^+ + 2}e\end{aligned} \tag{10}$$

During discharge the charge transport is shared unequally by the H^+ and HSO_4^- ions. To transport one electron requires μ H^+ ions and $(1-\mu)$ HSO_4^- ions, where μ is equal to 0.81 [5]. For an external transport of 2 electrons, the following processes are required per volume element of electrolyte [5].

$$\begin{aligned}&+\text{pole:}\\ &-\mathrm{HSO_4^-} - 3\mathrm{H^+} + 2\mathrm{H_2O} && -\text{from the reaction}\\ &\quad 2\mu\mathrm{H^+} && -\text{in due to the charge transport}\\ &-2(1-\mu)\mathrm{HSO_4^-} && -\text{out due to the charge transport}\\ &----------+\end{aligned} \tag{11}$$

$$\begin{aligned}&-(3-2\mu)\mathrm{H_2SO_4} + 2\mathrm{H_2O}\\ &-\text{pole:}\\ &-\mathrm{HSO_4^-} + \mathrm{H^+} && -\text{from the reaction}\\ &2(1-\mu)\mathrm{HSO_4^-} && -\text{in due to the charge transport}\\ &-2\mu\mathrm{H^+} && -\text{out due to the charge transport}\\ &----------+\\ &(1-2\mu)\mathrm{H_2SO_4}\end{aligned} \tag{12}$$

Therefore the decrease in acid per unit of charge transport at the positive and negative plates can be written as.

$$\left(\frac{\partial H}{\partial Q}\right)_+ = -\frac{(3-2\mu)}{2F} \tag{13}$$

$$\left(\frac{\partial H}{\partial Q}\right)_- = \frac{(1-2\mu)}{2F} \tag{14}$$

where F is Faraday's constant (approximately 96,500 C/mol). Using a value of 0.81 for μ returns a value of -7.15×10^{-6} mol/C at the positive plate and 3.21×10^{-6} mol/C for the negative plate [5].

The concentration at the positive plate decreases more rapidly than at the negative plate not only due to the extraction of H_2SO_4, but also because it is being diluted by the water formed during the reaction. The change in concentration at the positive electrode due to the addition of water can be estimated by the following equation [5].

$$\left(\frac{\partial H}{\partial Q}\right)_+ = -\{7.15 + 0.1865[C]\cdot(1-0.03[C])\} \times 10^{-6}\,\mathrm{mol/C} \tag{15}$$

where $[C]$ is the concentration of H_2SO_4 in mol/l. For the fairly small changes in concentration seen in lead–acid batteries, this value can be simplified to the constant value stated above.

When the above relations are substituted into the PDE

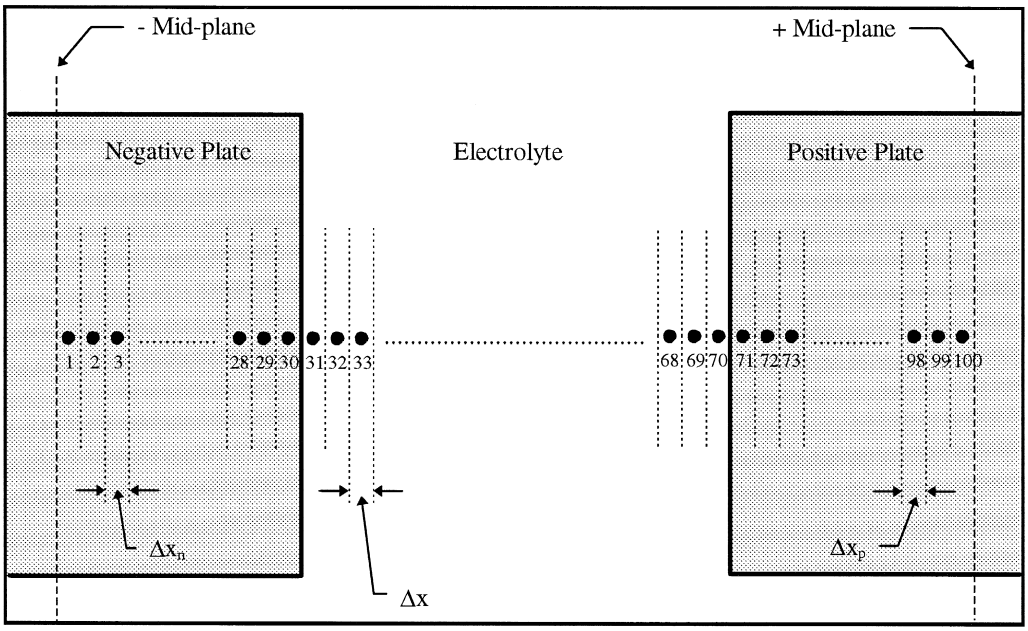

Fig. 1. Finite difference node arrangement.

in Eq. (3), we find the general finite difference equation inside the plates to be:

$$-\lambda_{p,n}C_{i-1}^{l+1}+2(\rho_{p,n}+\lambda_{p,n})C_i^{l+1}-\lambda_{p,n}C_{i+1}^{l+1}=\lambda_{p,n}C_{i-1}^{l}+2(\rho_{p,n}-\lambda_{p,n})C_i^{l}+\lambda_{p,n}C_{i+1}^{l}+K_{p,n}\dot{m}_i \quad (16)$$

where $\lambda_{p,n}=\dfrac{D_{p,n}\cdot\Delta t}{\Delta x_{p,n}^2}$ $K_{p,n}=\dfrac{2\Delta t}{A\Delta x_{p,n}}$ and the subscripts p and n refer to either the positive or negative plate.The specific diffusion rates, $D_{p,n}$, used above are calculated from:

$$D_{p,n}=D^*\cdot\rho_{p,n}=D\frac{\rho_{p,n}}{\tau} \quad (17)$$

Multiplying D^* by $\rho_{p,n}$ further reduces the diffusion rate in proportion to the reduced area (porosity) of the plate.

The two general finite difference equations derived above, Eqs. (5) and (16), cover all of the nodes in Fig. 1 except for the boundary nodes. Section 2.4 discusses each of the boundary conditions and derives the specific finite difference equation that applies to those nodes.

2.4. Boundary conditions

Referring to Fig. 1, it can be seen that boundary conditions exist at the nodes representing the center of the negative plate (1) and positive plate (100), the interface between the negative plate and electrolyte (30, 31), and the interface between the positive plate and electrolyte (70, 71). Each of these nodes requires a special finite difference equation. However, due to symmetry, each boundary node in the negative plate shares its boundary condition and derivation with its counterpart in the positive plate (e.g., 1 and 100, 30 and 71, 31 and 70). Hence, only the derivation of the negative plate nodes (1, 30, and 31) is discussed, but all equations are given.

2.5. Center of electrodes (nodes 1 and 100)

Node 1 occurs at the center of the negative plate as shown in Fig. 1. The imaginary node 0 occurs on the opposite side of the boundary. Due to symmetry about the midplane, there is no concentration gradient across this boundary and therefore no ion transfer. This relationship can be written for both plates at the beginning and end of the time increment as.

$$\text{Negative plate: } C_0^l=C_1^l \text{ and } C_0^{l+1}=C_1^{l+1} \quad (18)$$

$$\text{Positive plate: } C_{100}^l=C_{101}^l \text{ and } C_{100}^{l+1}=C_{101}^{l+1} \quad (19)$$

The above relationships in Eq. (18) can be substituted in Eq. (16) to eliminate the imaginary node 0. Making this substitution and collecting terms results in the boundary equation for node 1.

$$(2\rho_n+\lambda_n)C_1^{l+1}-\lambda_nC_2^{l+1}=(2\rho_n-\lambda_n)\times C_1^l+\lambda_nC_2^l+K_n\dot{m}_1 \quad (20)$$

Notice that the imaginary node 0 is no longer a part of the equation. Following the same derivation for the positive plate results in the related boundary equation for node 100.

$$-\lambda_pC_{99}^{l+1}+(2\rho_p+\lambda_p)C_{100}^{l+1}=\lambda_pC_{99}^l+(2\rho_p-\lambda_p)\times C_{100}^l+K_p\dot{m}_{100} \quad (21)$$

2.6. Electrode / electrolyte interface (nodes 30 and 71)

Node 30 is the last node within the negative plate and borders the electrolyte as shown in Fig. 2. Node N is an

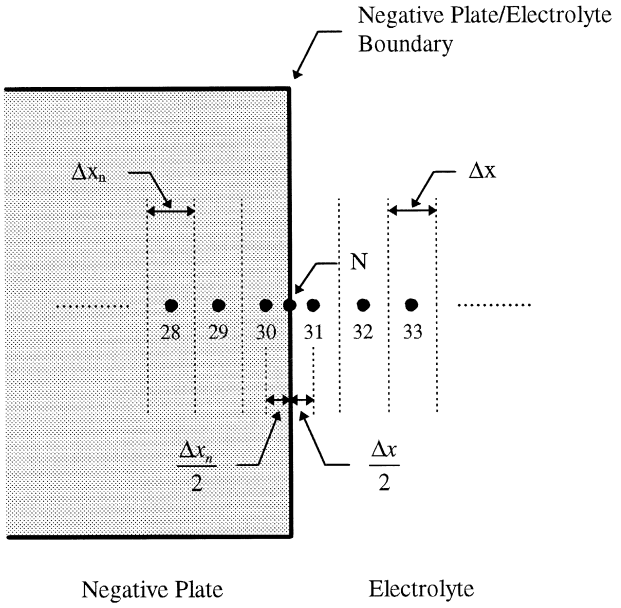

Fig. 2. Boundary condition at the negative plate/electrolyte interface (node 30).

imaginary node used to approximate the concentration, C_N, at the boundary between the negative plate and the electrolyte. Due to mass conservation it is assumed that the flux of ions on one side of the boundary is equal to the ion flux on the opposite side of the boundary. In mathematical terms, this can be written as.

$$J = -D_{\mathrm{n}} \frac{\partial C}{\partial x}\bigg|_{x_N = 0^-} = -D \frac{\partial C}{\partial x}\bigg|_{x_N = 0^+} \tag{22}$$

where $x_N = 0^-$ is the location just to the left of the boundary (inside the negative plate); $x_N = 0^+$ is the location just to the right of the boundary (in the electrolyte).Eq. (22) can be rewritten in terms of the nodes shown in Fig. 2 as.

$$D_{\mathrm{n}}\left(\frac{C_N - C_{30}}{\Delta x_{\mathrm{n}}/2}\right) = D\left(\frac{C_{31} - C_N}{\Delta x/2}\right) \tag{23}$$

The boundary concentration, C_N, can now be solved for in the above equation. After solving and simplifying the result is:

$$C_N = \frac{R_3}{2} C_{30} + \frac{R_4}{2} C_{31} \tag{24}$$

$$\text{where } R_3 = \frac{2 D_{\mathrm{n}} \Delta x}{D_{\mathrm{n}} \Delta x + D \Delta x_{\mathrm{n}}} R_4 = \frac{2 D \Delta x_{\mathrm{n}}}{D_{\mathrm{n}} \Delta x + D \Delta x_{\mathrm{n}}} \text{A} \quad \text{new}$$

second derivative in space is needed for this situation because of the different spacing at the boundary.

$$\frac{\partial^2 C}{\partial x^2} = \frac{1}{2}\left[\frac{\dfrac{\frac{1}{2}\left(C_{29}^{l} - C_{30}^{l}\right)}{\Delta x_n/2} - \dfrac{\left(C_{30}^{l} - C_N^{l}\right)}{\Delta x_n/2}}{\Delta x_n} + \frac{\dfrac{\frac{1}{2}\left(C_{29}^{l+1} - C_{30}^{l+1}\right)}{\Delta x_n/2} - \dfrac{\left(C_{30}^{l+1} - C_N^{l+1}\right)}{\Delta x_n/2}}{\Delta x_n}\right] \tag{25}$$

Eq. (25) can now be simplified by substituting in the equation for C_N from Eq. (24). This result is then inserted into Eq. (3) (the temporal derivative is unchanged) and with much algebra we arrive at the boundary condition for the last node in the negative plate, node 30.

$$\begin{aligned} &-\lambda_{\mathrm{n}} C_{29}^{l+1} + \left(-\lambda_{\mathrm{n}} R_3 + 2\rho_{\mathrm{n}} + 3\lambda_{\mathrm{n}}\right) C_{30}^{l+1} - \lambda_{\mathrm{n}} R_4 C_{31}^{l+1} \\ &\quad = \lambda_{\mathrm{n}} C_{29}^{l} + \left(\lambda_{\mathrm{n}} R_3 + 2\rho_{\mathrm{n}} - 3\lambda_{\mathrm{n}}\right) C_{30}^{l} \\ &\qquad + \lambda_{\mathrm{n}} R_4 C_{31}^{l} + K_{\mathrm{n}} \dot{m}_{30} \end{aligned} \tag{26}$$

Notice that if $D_{\mathrm{n}} = D$ and $\Delta x_{\mathrm{n}} = \Delta x$ in the above equation, then $R_3 = R_4 = 1$ and Eq. (26) simplifies to the general equation inside the negative plate, Eq. (16). This confirms the validity of the boundary equation and shows that it is merely a specialized case of the general equation.

Following a derivation similar to that of node 30 in the negative plate results in the boundary equation for the first node in the positive plate, node 71:

$$\begin{aligned} &-\lambda_{\mathrm{p}} R_1 C_{70}^{l+1} + \left(-\lambda_{\mathrm{p}} R_2 + 2\rho_{\mathrm{p}} + 3\lambda_{\mathrm{p}}\right) C_{71}^{l+1} - \lambda_{\mathrm{p}} C_{72}^{l+1} \\ &\quad = \lambda_{\mathrm{p}} R_1 C_{70}^{l} + \left(\lambda_{\mathrm{p}} R_2 + 2\rho_{\mathrm{p}} - 3\lambda_{\mathrm{p}}\right) C_{71}^{l} \\ &\qquad + \lambda_{\mathrm{p}} C_{71}^{l} + K_{\mathrm{p}} \dot{m}_{71} \end{aligned} \tag{27}$$

$$\text{where } R_1 = \frac{2 D \Delta x_{\mathrm{p}}}{D \Delta x_{\mathrm{p}} + D_{\mathrm{p}} \Delta x} \text{ and } R_2 = \frac{2 D_{\mathrm{p}} \Delta x}{D \Delta x_{\mathrm{p}} + D_{\mathrm{p}} \Delta x}.$$

2.7. Electrode / electrolyte interface (nodes 31 and 70)

The boundary condition for the first node in the electrolyte, node 31, is the same as that of the last node in the negative plate, node 30 (Eq. (22)). Therefore, the finite difference equation is developed in a very similar fashion. The difference results because node 30 is located inside the plate, and node 31 is located in the electrolyte. Fig. 2

shows the node arrangement used in deriving the boundary equation. Eq. (22) can be written for this node as.

$$D_{\mathrm{n}}\left(\frac{C_N - C_{30}}{\Delta x_{\mathrm{n}}/2}\right) = D\left(\frac{C_{31} - C_N}{\Delta x/2}\right) \tag{28}$$

We now solve for C_N as before and substitute it into the second spatial derivative. The second spatial derivative is then used with Eq. (4) which results in the boundary equation for the first node in the electrolyte, node 31.

$$-\lambda R_3 C_{30}^{l+1} + (-\lambda R_4 + 2 + 3\lambda) C_{31}^{l+1} - \lambda C_{32}^{l+1} = \lambda R_3 C_{30}^{l} + (\lambda R_4 + 2 - 3\lambda) C_{31}^{l} + \lambda C_{32}^{l} \tag{29}$$

where λ, R_3, and R_4 have been defined previously. Again, by letting $D_{\mathrm{n}} = D$ and $\Delta x_{\mathrm{n}} = \Delta x$, $R_3 = R_4 = 1$ and Eq. (29) simplifies to the general finite difference equation between the plates, Eq. (5).

The corresponding boundary equation for the last node in the electrolyte, node 70, is.

$$-\lambda C_{69}^{l+1} + (-\lambda R_1 + 2 + 3\lambda) C_{70}^{l+1} - \lambda R_2 C_{71}^{l+1} = \lambda C_{69}^{l} + (\lambda R_1 + 2 - 3\lambda) C_{70}^{l} + \lambda R_2 C_{71}^{l} \tag{30}$$

2.8. Matrix solution

Writing the finite difference equations for each of the 100 nodes results in a system of equations which can be put into the following Jacobian matrix form:

$$[\mathbf{A}]\{\boldsymbol{C}\} = \{\boldsymbol{K}\} \tag{31}$$

where [**A**] is a 100×100 tridiagonal coefficient matrix; $\{\boldsymbol{C}\}$ is a 100×1 vector of the node concentrations; $\{\boldsymbol{K}\}$ is a 100×1 vector based on the concentrations of the previous time step.

Once all of the finite difference equations have been put into matrix form, the system of equations can be solved simultaneously using Jacobian matrix methods. During each time step, the new concentration vector, $\{\boldsymbol{C}\}$, must be determined. Using matrix algebra, the above equation can be written as:

$$\{\boldsymbol{C}\} = [\mathbf{A}]^{-1}\{\boldsymbol{K}\} \tag{32}$$

Normally, solving Eq. (32) would require extensive matrix algebra to invert the 100×100 [**A**] matrix. However, due to the form of the finite difference equations, [**A**] takes the form of a tridiagonal matrix. This is a common matrix form found in many engineering problems and therefore fast, efficient methods have been developed [17,18] to solve for the relevant terms in this equation while ignoring all of the zero terms. This eliminates the need to invert the large [**A**] matrix.

At the beginning of the discharge, all of the nodes are at the same concentration. To sustain the discharge current, all nodes are discharged equally. However, after the first time step, the acid concentration differs from node to node. The electrolyte between the plates begins to diffuse into the plates such that the nodes closer to the plate surface have a higher concentration than those further inside. The model is based upon the idea that the nodes will discharge in the order of their acid concentration. This means that the node with the highest concentration will discharge first, followed by the node with the second highest concentration, etc. To control the discharge, the model uses a sorting routine for both the positive and negative plates. These routines sort the nodes from the highest concentration to the lowest.

During subsequent time steps, the node with the highest concentration (the reaction node) is discharged to the node with the second highest concentration. The resulting current is compared with the specified discharge current. If these currents are equal, then the program proceeds to the next time step by diffusing electrolyte into the plates and calculating the new concentration array using Eq. (32). If the discharge current has not been met, the node with the next lower concentration becomes the reaction node. All nodes with concentrations higher than the reaction node are then discharged to the reaction node and the current drawn from each discharged node is summed to determine if the discharge current is supported. Whenever the discharge current is not supported, the reaction node is changed to the next lower concentration and the process is repeated. Once the discharge current is met, the model proceeds to the next time step and the concentration array is updated. If the reaction node must be moved to the lowest concentration in the plate, all of the nodes are reacted to the same concentration. If the resulting current is still insufficient, then all of the nodes are discharged to a concentration level that will support the discharge current.

During every time step, each node is also checked to see how much active material has reacted. During discharge the conductive active material (PbO or PbO_2) is converted to nonconductive $PbSO_4$. Metzendorf's critical volume fraction hypothesis [1] states that once the ratio of reacted to unreacted material, known as the critical volume fraction, reaches a certain point, the reaction stops. To account for this condition in the model, the ratio of material reacted at any node is limited to the specified critical volume fraction by using the following equation.

$$\sum_{l=1}^{T} \Delta I_i^l \Delta t \le \eta C_{\mathrm{s}} \tag{33}$$

where ΔI_i is the current at each individual node, T is the total discharge time, Δt is the time step, η is the critical volume fraction, and C_{s} is the theoretical stoichiometric capacity associated with each node.

As soon as any node reaches its critical volume fraction, the node is 'turned off' by setting the $\dot{m}$ term for that node to zero. This means that this node can no longer contribute to the discharge current. As a result of the node

being turned off, the $\{\boldsymbol{K}\}$ vector is also altered to reflect this change during future time steps.

By knowing the concentrations at each node and for each time step, concentration profiles can be drawn. Examples are given in Section 3. The concentrations can also be used to determine the cell voltage during each time step by using the Nernst equation [19]:

$$E = E^{\circ} - \frac{2.30\,RT}{nF}\log_{10} Q \tag{34}$$

where E° is the equilibrium potential, R is the gas constant, T is the absolute temperature, n is the number of electrons transferred during the reaction, F is Faraday's number, and Q is the reaction quotient. By applying this equation to the positive and negative electrodes at 313 K (40°C), the following equations result.

$$E_{+} = E^{\circ}_{+} + 0.031 \cdot \log_{10}\left(\left[\mathrm{H}^{+}\right]^{3}\left[\mathrm{HSO}_{4}^{-}\right]\right) \tag{35}$$

$$E_{-} = E^{\circ}_{-} - 0.031 \cdot \log_{10}\frac{\left[\mathrm{H}^{+}\right]\left[\mathrm{HSO}_{4}^{-}\right]}{\left[\mathrm{H}^{+}\right]^{2}} \tag{36}$$

By noting that the equilibrium potential of the positive electrode, E°_{+}, is 1.602 V and that $[\mathrm{H}^{+}]$ and $[\mathrm{HSO}_{4}^{-}]$ are nearly equal to the total acid concentration, $[C]$, Eq. (35) can be simplified to.

$$E_{+} = 1.602 + 0.124 \cdot \log_{10}[C] \tag{37}$$

Referring to Eq. (36), the potential of the negative electrode, E_{-}, has hardly any dependence on the acid concentration. Therefore it is nearly constant and equal to E°_{-} which is -0.303 V. The positive and negative potentials can be combined to get the total cell potential by using the following expression.

$$E = E_{+} + E_{-} \tag{38}$$

The final equation used to determine the cell potential is found by substituting E_{+} and E_{-} into Eq. (38):

$$E = 1.905 + 0.124 \cdot \log_{10}[C] \tag{39}$$

where $[C]$ is the acid concentration in mol/l. The minimum concentration in the positive plate is used in the above equation to determine the cell potential at each time step. When the cell potential drops to a pre-determined voltage (usually 1.75 V), the model discontinues the discharge process. By keeping track of the potential during the entire discharge, voltage vs. time curves can be constructed. Section 3 uses these curves as a method to compare the predicted model data to experimental data.

3. Model verification

In order to run the model developed in Section 2.8, a number of physical parameters are needed. These parameters are determined by the plate type, cell design, and other factors. Section 3.1 lists and discusses these parameters. In Sections 3.1 and 3.2, the computer model is used to simulate commercial standard positive and negative plates. The results are verified by comparing them to experimental data. The experimental data for these plates was gathered by Edwards and Srikanth [16]. The model is also used to predict the behavior of plates with glass microsphere paste additives. These results are then compared with additional experimental data gathered by Edwards and Srikanth [16].

Table 1
Model parameters used for the simulation of a commercial cell

Plate type	Commercial
Positive plate	
Plate thickness (cm)	0.244
Plate area (cm^2)	114.2
Grid volume (cm^3)	1.768
PAM weight (g)	83
Critical volume fraction	60%
Percent porosity	34%
Glass microsphere additives (volume percent)	0%
Stoichiometric capacity (A·h)	18.6
Negative plate	
Plate thickness (cm)	0.185
Plate area (cm^2)	114.2
Grid volume (cm^3)	1.768
Critical volume fraction	60%
Percent porosity	34%
Miscellaneous	
Distance between plates (cm)	0.254
Initial acid concentration (mol/liter)	5.04
Cutoff voltage (volts)	1.75
Electrical resistance of the cell (Ω)	-0.026
Initial voltage correction (volts)	2.13773
Diffusion constant of H_2SO_4 (cm^2/sec)	2.590 e^{-5}

3.1. Model parameters

The parameters needed in the model include variables that relate the physical dimensions of the plates as well as variables that control the diffusion and conductivity behavior of the paste. Table 1 lists the set of parameters used in Section 3.2 to model the commercial standard plates.

The diffusion behavior of the cell is governed by a number of the model parameters. The plate dimensions and porosity are used to determine the amount of electrolyte stored within the plates. The electrolyte inside the plates is

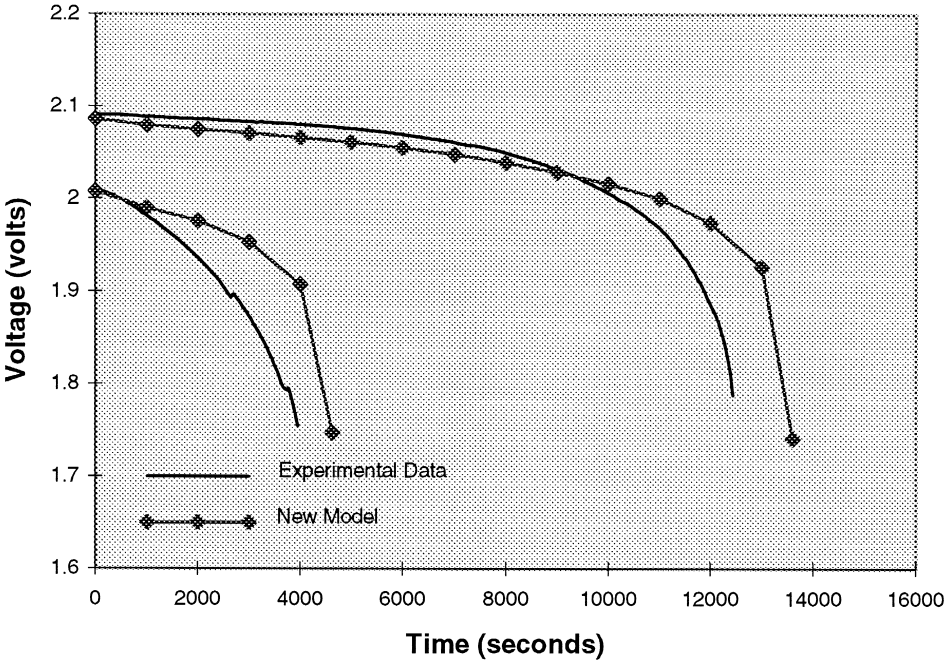

Fig. 3. Comparison of voltage vs. time curves for standard commercial cells discharged at various rates (0.023 and 0.059 A/g).

important, especially at high rates, because this electrolyte does not need to diffuse to react. The acid diffusion constant of 2.590 e^{-5} cm^2/s is based on low acid concentrations at approximately 38°C. The low concentration diffusion constant is used to more closely approximate the cell behavior at the end of discharge.

The conductivity parameters include the electrical resistance of the cell and the open circuit voltage, which

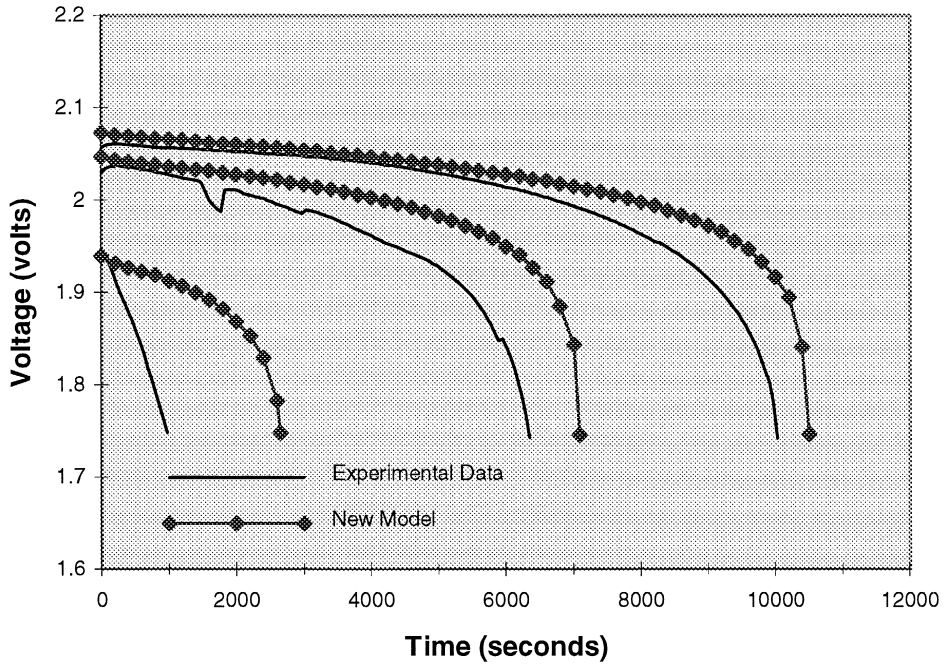

Fig. 4. Comparison of voltage vs. time curves for standard commercial cells discharged at various rates (0.03, 0.041 and 0.09 A/g).

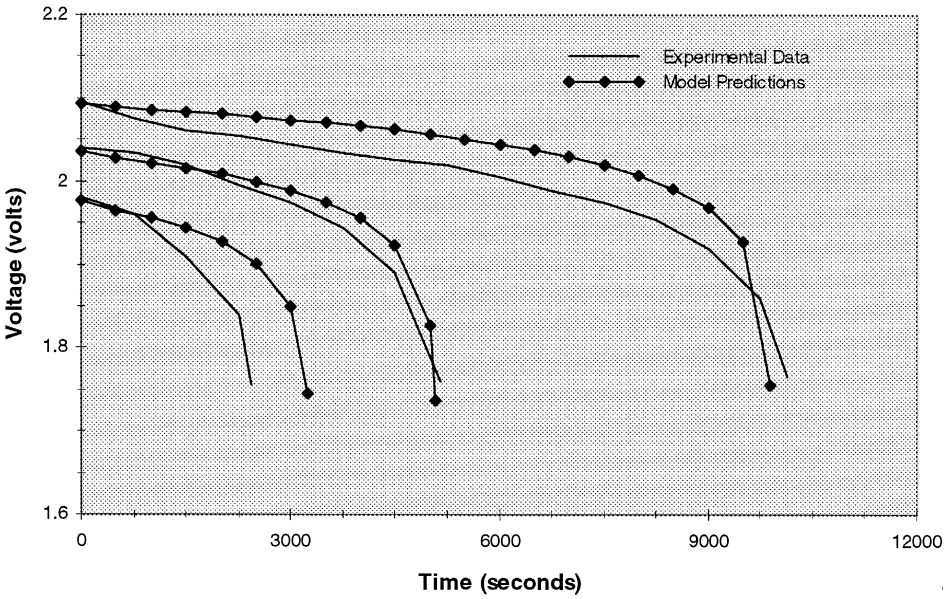

Fig. 5. Comparison of voltage vs. time curves at various discharge rates (0.086, 0.060, and 0.034 A/g) for positive plates containing 19.5% by volume nonconductive glass microspheres.

depends on the initial acid concentration and the activity coefficients. The values listed for these variables also take into account the resistance of the test equipment in order to accurately reproduce the experimental conditions. Another important conductivity parameter is the critical volume fraction which can be affected by the amount of paste additives. This critical volume fraction is determined from another computer model developed specifically for this purpose [2]. The discharge is also dependent on the cutoff voltage, which determines when the reaction is stopped.

3.2. Experimental comparisons

Figs. 3 and 4 compare voltage vs. time curves produced by the new model with experimental data previously reported by Edwards and Srikanth [16]. The data has been split into two different figures for clarity. The model

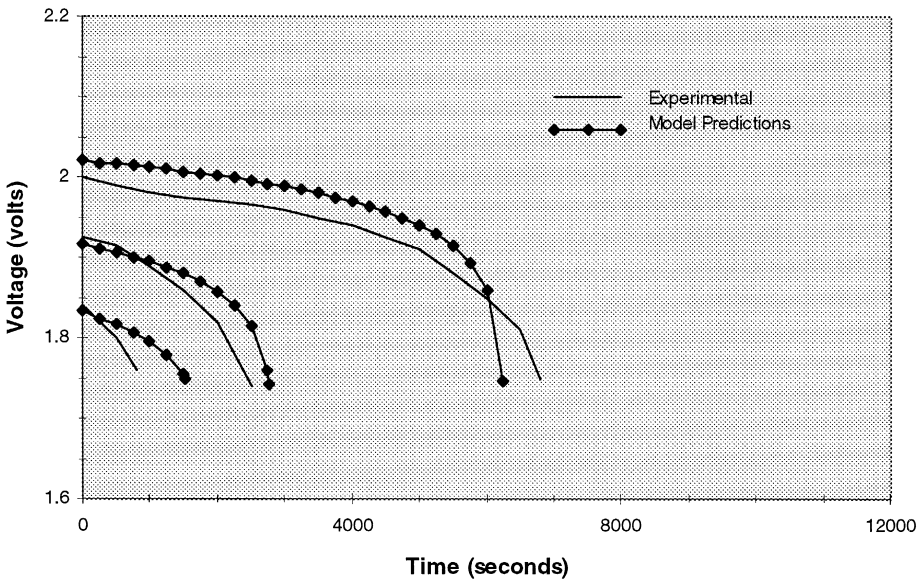

Fig. 6. Comparison of voltage vs. time curves at various discharge rates (0.142, 0.099, and 0.057 A/g) for positive plates containing 34.0% by volume nonconductive glass microspheres.

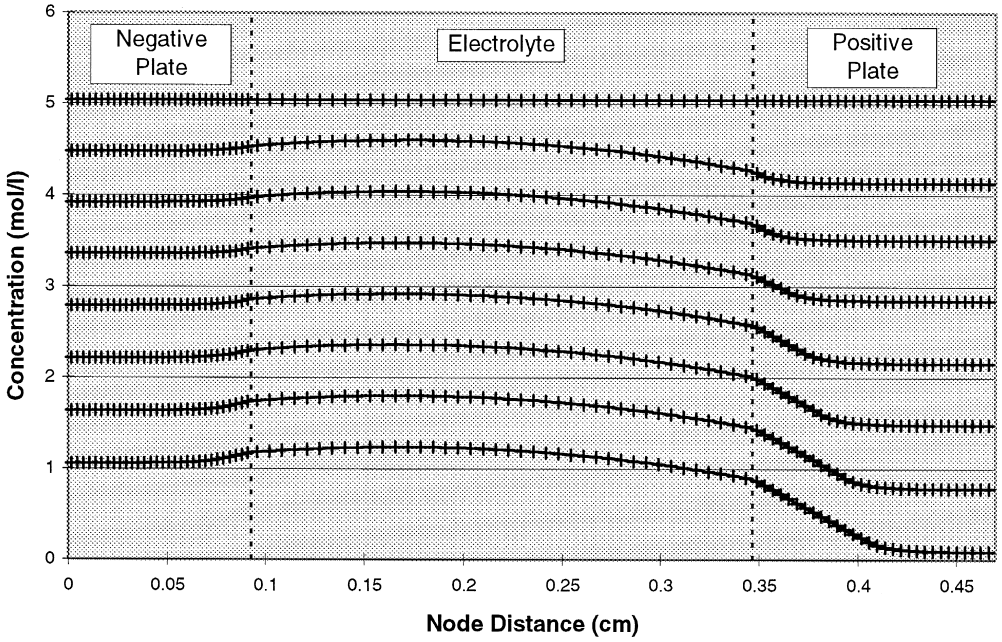

Fig. 7. Concentration profiles of a standard commercial cell discharged at 0.041 A/g plotted every 1000 s.

allows the time step and time between data points to be specified independently. This allows the use of a small time step (1 s) for high accuracy, while reducing the large amount of data produced during a slow discharge. As the figures show, the model predicts the test results fairly accurately, especially at the medium to low rates. At higher rates, the model tends to overestimate the capacity of the cell. This is possibly attributed to an oversimplification of the cell resistance by neglecting the porosity and resistance of the separator.

The model can also simulate the effects of paste additives. To validate the model's capability to accurately simulate these effects, model predictions are compared to experimental additive data gathered by Edwards and Srikanth [16]. Fig. 5 gives voltage vs. time curves for a positive plate containing 19.5% by volume of nonconduc-

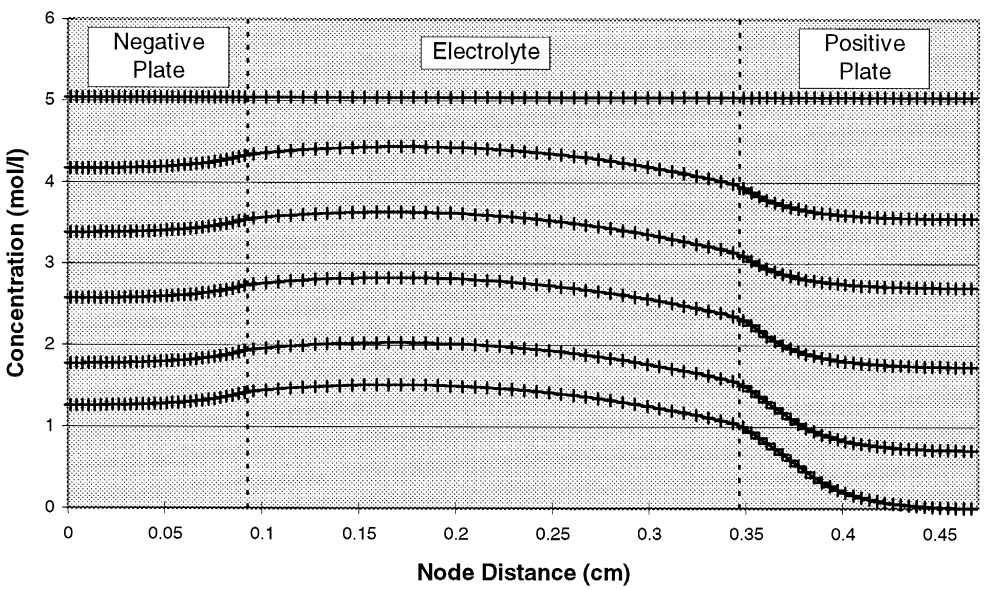

Fig. 8. Concentration profiles of a standard commercial cell discharged at 0.059 A/g plotted every 1000 s.

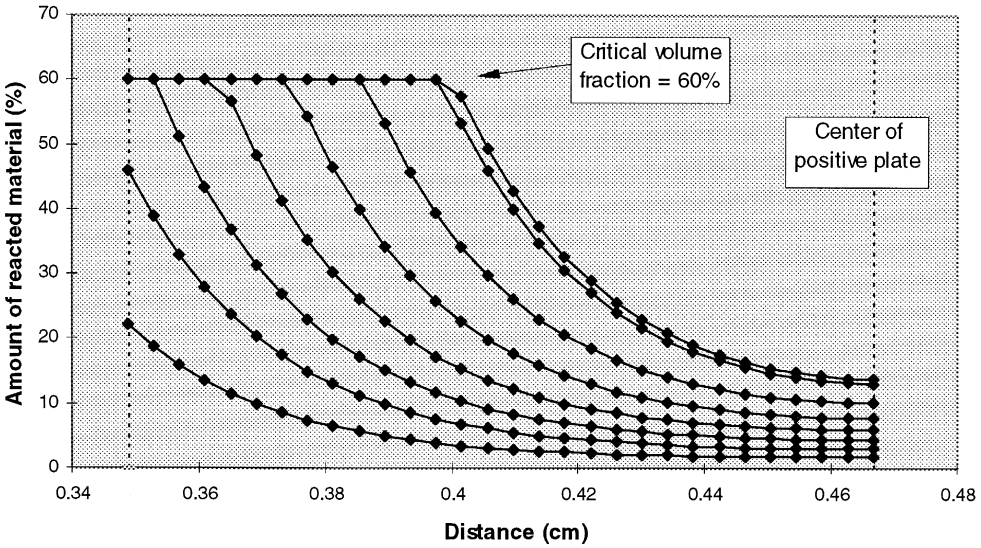

Fig. 9. Percentage of positive active material reacted as a function of distance inside the positive plate after every 2000 s.

tive glass microspheres. The discharge rates shown in the figure are 0.086, 0.060, and 0.034 A/g. Both the computer generated curves and the experimental data are included in the figure. As the reader can see, the computer generated curves provide a reasonable representation of the experimental curves.

Fig. 6 shows various voltage vs. time curves for a plate containing 34.0% by volume of non-conductive glass microspheres. The figure is similar to Fig. 5 and compares the model predictions to experimentally gathered data at discharge rates of 0.142, 0.099, and 0.057 A/g. Again, the computer predictions follow the experimental curves fairly closely.

The model can also be used to estimate the acid distribution within a cell. Fig. 7 shows the model prediction of acid concentrations throughout a standard cell every 1000 s during the 0.041 A/g discharge shown in Fig. 4. The *x*-axis represents the node distance starting from the midplane of the negative plate. The *y*-axis indicates the concentration in mol/l for each node. The beginning of the discharge starts with equal concentrations at each node (the top line). As the discharge progresses, the electrolyte in the plates is consumed, while the electrolyte between the plates diffuses into the plates. This causes the concentration to drop throughout the entire cell. The steeper concentration gradients at the positive plate reflect the conditions derived earlier in Eqs. (13) and (14).

Fig. 8 shows a concentration profile similar to that of Fig. 7. However, the discharge rate has been increased to 0.059 A/g. The time between curves is again 1000 s. The reader will notice that the concentrations drop more rapidly, reflecting the higher discharge rate. Between the plates, the concentrations stay higher because there is insufficient time for the electrolyte to diffuse into the plates before the reaction stops.

The model output can also be used to develop $PbSO_4$ distribution curves like those shown in Fig. 9. This curve plots the amount of material that has reacted at each node in the positive plate every 2000 s. This curve is for a standard commercial cell discharged at 0.023 A/g as shown in Fig. 3. The vertical axis represents the percentage of active material that has reacted within the positive plate. The horizontal axis shows the position within the positive plate starting at the electrolyte/electrode interface, and ending at the midplane of the positive plate. The reader can see that the nodes near the surface of the plate are reacting to their critical volume fraction of 60%. As the discharge continues, the reaction continues towards the center of the plate. The nodes cannot react more than their critical fraction because they have been 'turned off' by the program, as discussed earlier. The shape of the curve shown in Fig. 9 is similar to experimental lead sulfate distribution curves reported by Bode [4] and Simonsson [3].

4. Summary and conclusions

The model presented in this paper uses finite difference equations to predict the behavior of lead–acid batteries. The model includes both diffusion and conductivity parameters including the critical volume fraction, porosity of the electrodes, cell resistance, and initial acid concentration. These parameters are used in the finite difference equations to model the behavior of both electrodes as well as the electrolyte between them. A sorting routine is used by

the model to estimate where the active material will discharge within the electrodes at each time interval. This routine also uses the critical volume fraction to limit the total amount of material reacting. The predicted results compare reasonably well with experimental data, especially at medium to low rates. The present model predicts battery capacity over a wide range of discharges and can be used as an effective tool for designing batteries, including those for EV and HEV applications.

References

[1] H. Metzendorf, J. Power Sources 7 (1982) 281–291.
[2] P.W. Appel, Masters Thesis, Univ. of Idaho, Moscow, ID, USA, 1991.
[3] D. Simonsson, J. Electrochem. Soc. 120 (1973) 151–157.
[4] H. Bode, Lead–Acid Batteries, Wiley, New York, 1977.
[5] W. Stein, Thesis, Rogowski-Institut für Elktrotechnik der Technischen Hochshule, Aachen, Germany, 1959.
[6] P. Horvàth, P. Jedlovszky, M. Benedek, J. Power Sources 8 (1982) 41–54.
[7] P. Ekdunge, D. Simonsson, J. Appl. Electrochem. 19 (1989) 136–141.
[8] P. Ekdunge, J. Power Sources 46 (1993) 251–262.
[9] A. Winsel, E. Voss, U. Hullmeine, J. Power Sources 30 (1990) 209–226.
[10] A. Winsel, E. Bashtavelova, J. Power Sources 46 (1993) 211–218.
[11] D.B. Edwards, P.W. Appel, J. Power Sources 38 (1992) 281–286.
[12] J.P. Pohl, W. Schendler, J. Power Sources 6 (1981) 245–250.
[13] P.W. Appel, Dissertation, Univ. of Idaho, Moscow, ID, USA, 1994.
[14] P.S. Gill, Masters Thesis, Univ. of Idaho, Moscow, ID, USA, 1995.
[15] R.L. Cantrell, Masters Thesis, Univ. of Idaho, Moscow, ID, USA, 1996.
[16] D.B. Edwards, V. Srikanth, J. Power Sources 34 (1991) 217–232.
[17] S.C. Chapra, R.P. Canale, Numerical Methods for Engineers, 2nd edn., McGraw-Hill, New York, 1988.
[18] W.H. Press, B.P. Flannery, S.A. Teukolsky, W.T. Vetterling, Numerical Recipes in Pascal, Cambridge Univ. Press, New York, 1989, pp. 48–49.
[19] Brown, Lemay, Bursten, Chemistry: The Central Science, pp. 739–740.